Low Cost AIP Design in 5G Flexible Antenna Phase Array System Application

Wei-Shin Tung [1], Wei-Yuan Chiang [2],[*], Chih-Kai Liu [1], Chiung-An Chen [2],[*], Pei-Zong Rao [1], Patricia Angela R. Abu [3], Wan-Ming Chen [1], Faisal Asadi [2] and Shih-Lun Chen [4],[*]

[1] Shenzhen Jaguar Wave Technology Co. Ltd., Shenzhen 518103, China; Weishin.tung@jaguarwave.com (W.-S.T.); chihkai.liu@jaguarwave.com (C.-K.L.); peizong.rao@jaguarwave.com (P.-Z.R.); Maxwell.chen@jaguarwave.com (W.-M.C.)

[2] Department of Electrical Engineering, Ming Chi University of Technology, New Taipei City 24301, Taiwan; asadifaisal@gmail.com

[3] Department of Information Systems and Computer Science, Ateneo de Manila University, Quezon City 1108, Philippines; pabu@ateneo.edu

[4] Department of Electronic Engineering, Chung Yuan Christian University, Taoyuan City 32023, Taiwan

[*] Correspondence: jameschiang@mail.mcut.edu.tw (W.-Y.C.); joannechen@mail.mcut.edu.tw (C.-A.C.); chrischen@cycu.edu.tw (S.-L.C.)

Abstract: In this paper, a low cost 28 GHz Antenna-in-Package (AIP) for a 5G communication system is designed and investigated. The antenna is implemented on a low-cost FR4 substrate with a phase shift control integrated circuit, AnokiWave phasor integrated circuit (IC). The unit cell where the array antenna and IC are integrated in the same plate constructs a flexible phase array system. Using the AIP unit cell, the desired antenna array can be created, such as 2×8, 8×8 or 2×64 arrays. The study design proposed in this study is a 2×2 unit cell structure with dimensions of 18 mm $\times$ 14 mm $\times$ 0.71 mm. The return loss at a 10 dB bandwidth is 26.5–29.5 GHz while the peak gain of the unit cell achieved 14.4 dBi at 28 GHz.

Keywords: phase array antenna; antenna in package; 28 GHz antenna

1. Introduction

Antenna technology is the latest breakthrough in design to accelerate cellular networks that aims to optimize the communication system in terms of smoothness and cost of the communications itself. Along with the development of the cellular network, currently the newest generation technology of the networks has arrived at the fifth generation (5G) network. The success of the 5G network paved its way to research for the newest technology product and to provide the best communication platform [1,2]. The 5G internet has become the center of research on how to improve its capabilities and novelty of the technology itself. The design of the Antenna in Package (AIP) is one field of research of 5G technology that can be improved to maximize the capabilities and functionalities of the technology [3].

The proposed research aims to optimize the bandwidth capabilities of the 5G technology by designing the AIP with models that exhibit low-cost array antenna design. The recent research on this field performed optimization of the 5G technology through space-frequency index modulation, spectral, energy, and economic fields [4,5]. On the other hand, many research also explored optimizing the scalability of the bandwidth of the 5G communication network. The first research was from K. Kibaroglu et al. [6] that has successfully designed a simple model 32-element (4×8) working at 28 GHz on the phased-array transceiver for 5G communication technology based on a 2×2 beamformer core chips. The research has achieved an effective isotropic radiated power (EIRP) of 43 dBm at P1dB, and the final state-of-art data rate was achieved in 1.0–1.6 Gb/s in a single beam using 16-QAM.

Similar research on improving the 5G technology network in a different area is conducted by J. Park et al. They improved the concept of the 5G technology through the use of the invisible Antenna-on-Display (AoD) that has been successful in the millimeter-wave for the cellular network. The invisible concept was designed and fabricated in a 1 × 8 optically invisible array that exhibits a 66.6 dBi boresight gain that operate at 28 GHz, which is still capable of maintaining 88% of the optical transparency. On the other side, A. M. Pawan Kumar et al. designed a quad-port wide-band multiple-input-multiple-output (MIMO) that integrated the wide Axial-ratio concept. This was successfully designed in a FR-4 dielectric substrate with size 45 × 45 × 1.6 mm^3. Moreover, the design of the proposed MIMO concept showed a 3-dB ARBW of 52% (3.8–6.5 GHz) and an impedance bandwidth (S11 ≤ −10 dB) of 144% (2.2–13.5 GHz) [7,8].

G. F. Hamberger et al. proposed an antenna array with a planar dual-polarized microstrip 1-D-Beamforming for the 24 GHz band. Simulation results showed that it could operate in a frequency of over 500 MHz. Similar work proposed a power-efficient multiband planar USB dongle antenna for a wireless sensors network. A USB dongle antenna was designed to work with three frequencies bands namely, 2.30–2.69 GHz, 3.40–3.70 GHz, and 5.15–5.85 GHz. At the end of the research, the efficiency of power consumption in the looping process has significantly improved [9–11].

The spread of virus and influenza in recent years required the monitoring of physiological signals without contact to the subjects, which is of the utmost priority. The wireless body sensor networks (WBSNs) [12,13] overcome the difficulties of high risk infecting. Furthermore, C.A. Chen et al. provided a low power [14] and efficient compression algorithm [15] to increase the effectiveness of communication data without any loss. Body signals with noise are easy to confuse the diagnosis and misjudge the symptom is another challenge. A filter with a reconfigurable clock [16] was designed for WBSNs with better noise filtering therefore acquiring smooth signals. With the advancement of both medical imaging and compressors, S.H. Chen et al. [17,18] used fuzzy decision and resolution to improve the rate of image compression. Moreover, a central control unit and cost-efficient WBSNs systems were required in a micro control unit implementation [19]. Moreover, the modularized device brings a lot of convenience on combining the system and can simplify the design of many other functional devices, like the wireless transmission of medical data by a wearable device [20]. These previous works contributed to the efficiency of the designs and real-time data implementations to wireless communication devices.

This paper expands and continues previous studies and proposes an improvement in the design of the AIP that is a low-cost 28 GHz AIP for the 5G communication system that is based on 2 × 2 beamformer core chips. The next sections present the phased-array architecture of the unit cells, the analysis system for the elements array, and circuit blocks. Section 4 presents and discusses the results and performance of the proposed design. In this study, the frequency band of the antenna focuses on the n257 band (26.5–29.5 GHz) [21].

2. Patch Antenna Design

In this study, the micro strip patch antennas constructed the array system. The patch antenna is a kind of a resonant antenna that is like a resonant cavity. One important parameter of a resonant cavity is its quality factor (Q_0), which is defined as shown in Equation (1) [22].

$$Q_0 \equiv \omega \frac{2W_e}{P_l} \tag{1}$$

where ω is the frequency, W_e is the stored energy in the resonant cavity, and P_l is the power loss of the resonant cavity. There are three kinds of losses in the resonant antenna namely radiation loss (P_{rad}), dielectric loss (P_d), and conducted loss (P_c). The formula is shown in Equation (2).

$$\frac{1}{Q_0} = \frac{P_{rad}}{2\omega W_e} + \frac{P_d}{2\omega W_e} + \frac{P_c}{2\omega W_e} = \frac{1}{Q_{rad}} + \frac{1}{Q_d} + \frac{1}{Q_c} \tag{2}$$

The antenna efficiency can be enhanced when the dielectric loss is reduced. This is due to the antenna efficiency (ξ), as shown in Equation (3) that is proportional to Q_0 when the conducted loss is fixed in the critical coupled condition.

$$\xi = \frac{P_{rad}}{P_l} \propto \frac{Q_0}{Q_{rad}} \qquad (3)$$

This study used an air-filled cavity structure to design the patch antenna on a standard FR4 substrate [23]. This design constructed a metal patch that was located on the FR4 substrate with the open air cavity. The reference ground used the copper layer on the carrier board as illustrated in Figure 1. This design can reduce the dielectric loss and enhance the patch antenna performance with better radiation efficiency. The dielectric constant of air was 1.0006 and the loss tangent of air was 0, which can enhance the patch antenna performance with better radiation efficiency. The top and cross section views are shown in Figure 2.
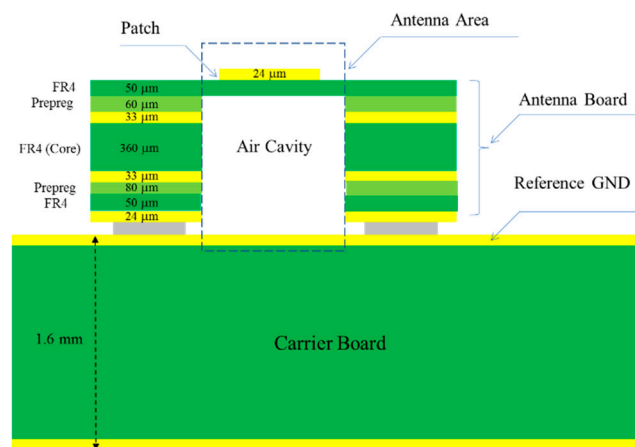

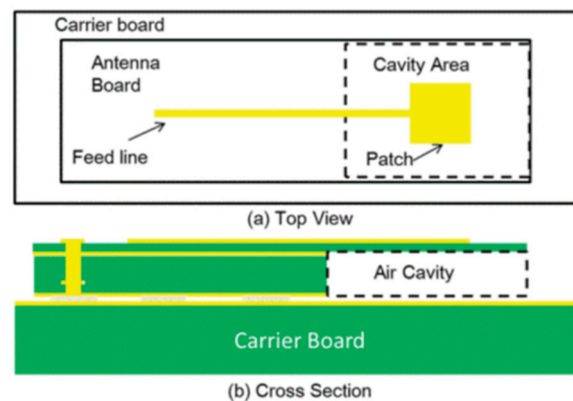**Figure 1.** The structure of the patch antenna with air cavity.

Figure 2. (**a**) Top view and (**b**) cross section view of the patch antenna.

The return loss and radiation efficiency of the patch antenna are presented in Figure 3. Figure 3a illustrates that the return loss of the patch antenna with air cavity is better than 10 dB at 26.5–29.5 GHz. Figure 3b presents the radiation efficiency of the two types of antenna where the radiation efficiency of the patch antenna with air cavity was 92% while the radiation efficiency of patch antenna without air cavity was 66.25% at 28 GHz. The radiation efficiency was enhanced by 25.75% at 28 GHz. The maximum radiation efficiency of the patch antenna with air cavity was 93.28% while the maximum radiation efficiency of patch antenna without air cavity was 77.25%. The radiation efficiency was enhanced by 16.03%.
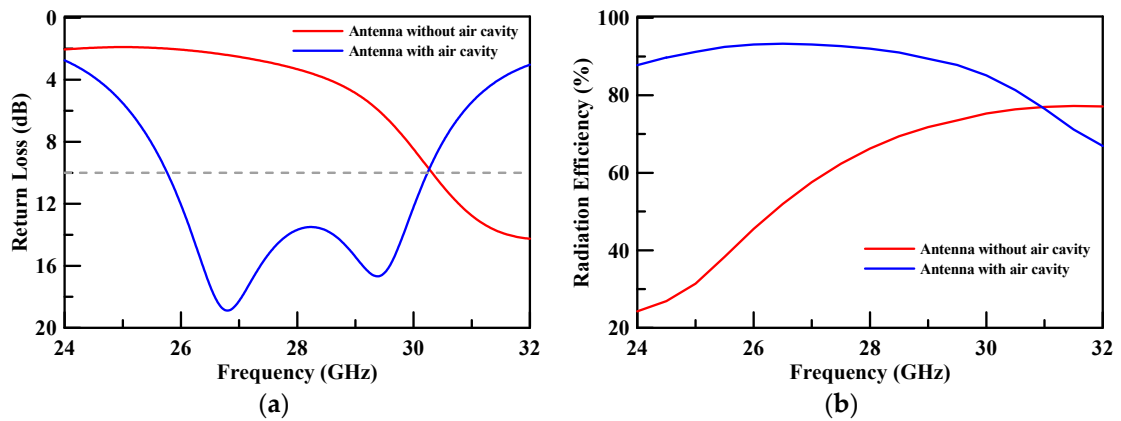
Figure 3. (**a**) The return loss and (**b**) the radiation efficiency of the patch antenna.

3. Array Antenna Design

The operation frequency band of the 5G system achieves the Ka-band. A small wavelength, small beam width, and high atmospheric attenuation are the shortcomings of this frequency band while its great advantages are its larger bandwidth and higher data rate. The multiple antenna techniques (MTA) is the solution that can solve wave shadowing of millimeter wave propagation [24]. The array antenna is an important development. The array antenna is composed of antennas that are arranged periodically as illustrated in Figure 4. The beam main lobe can be tilted by changing the phase of the antennas, which is called the beam steering technique.
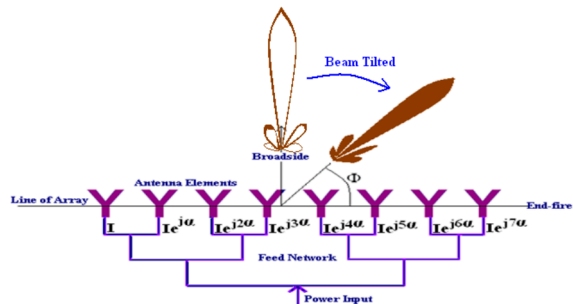

Figure 4. Beam steering/scanning antenna array [24].

In this study, the four patch antennas constituted a 2 × 2 array antenna as shown in Figure 5. An AnokiWave phasor IC was set at the same side with the patch antennas. Such an arrangement makes the array antenna become a complete system. This modular system is more flexible and expandable, which is widely known as the Antenna-in-Package (AIP).
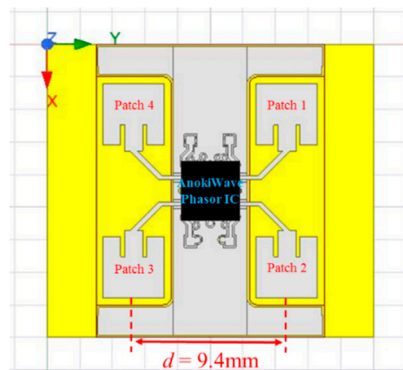

Figure 5. The structure of proposed array antenna with phasor IC.

The antenna spacing d is an important parameter in the design of the array antenna. In Figure 6, the ideal maximum array directivity (D) of a 2 × 2 array antenna is 6 dBi [25]. Basically, the single antenna gain (G) as shown in Equation (4) is proportional to the directivity of a single antenna. In fact, the antenna efficiency of each element does not need to be considered when taking into account the array gain. The array gain is equal to the array directivity. In this study, the estimated array gain is 5–6 dBi. Otherwise, the maximum scan angle must satisfy the condition in Equation (5). The θ_{max} is the maximum angle to which the array can be steered. The steering can be reckoned by Equation (5). The maximum angle is listed in Table 1 with an operating frequency of 28 GHz.

$$G_{single\ antnna} = \xi \cdot D_{single\ antenna} \tag{4}$$

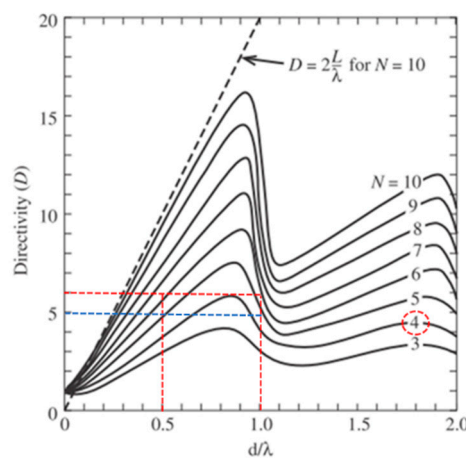$$\frac{d}{\lambda} \leq \frac{1}{1 + |\sin \theta_{max}|} \tag{5}$$

Figure 6. Directivity as a function of antenna spacing for a broadside array of isotropic elements [25].

The ideally maximum steering of the array antenna was ±90°. With that the antenna spacing was half the wavelength. In this study, the minimum spacing was 9.4 mm since the phasor IC was set at the center of the proposed array antenna. The maximum steering of the proposed array antenna approached ±10°.

Table 1. Maximum scan angle with different antenna spacing.

Maximum Angle θ_{max} (degree)	Wavelength λ at 28 GHz (mm)	Antenna Spacing d (mm)
10	10.71	9.13
20	10.71	7.98
30	10.71	7.14
40	10.71	6.52
50	10.71	6.07
60	10.71	5.74
70	10.71	5.52
80	10.71	5.40

The measured return loss of the simulated 2 × 2 array antenna of each port was better than 10 dB at an operating frequency of 26.5–29.5 GHz as shown Figure 7. The simulation results of each port were highly consistent, which is due to the structure of the array antenna that is in symmetry. The antenna peak gain was 14.4 dBi as shown through m1 in Figures 8 and 9. The 3 dB beam width that is shown through m2 and m3 on Figures 8 and 9, respectively, was 26°. The comparison of the simulation results of the single antenna and the array antenna is shown in Figure 10. The array gain was 5.78 dB, which was consistent with the estimative value.
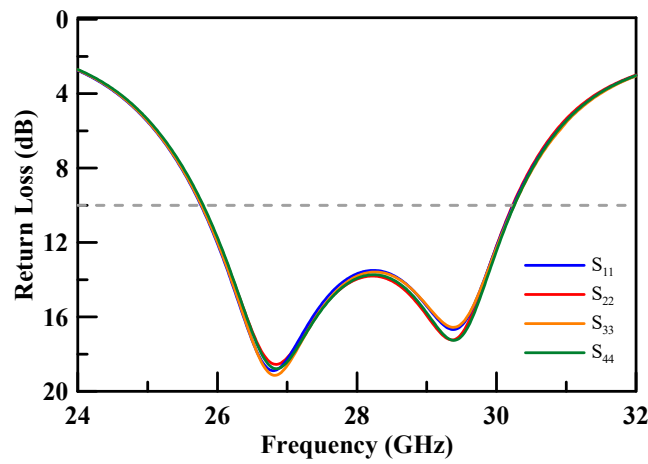
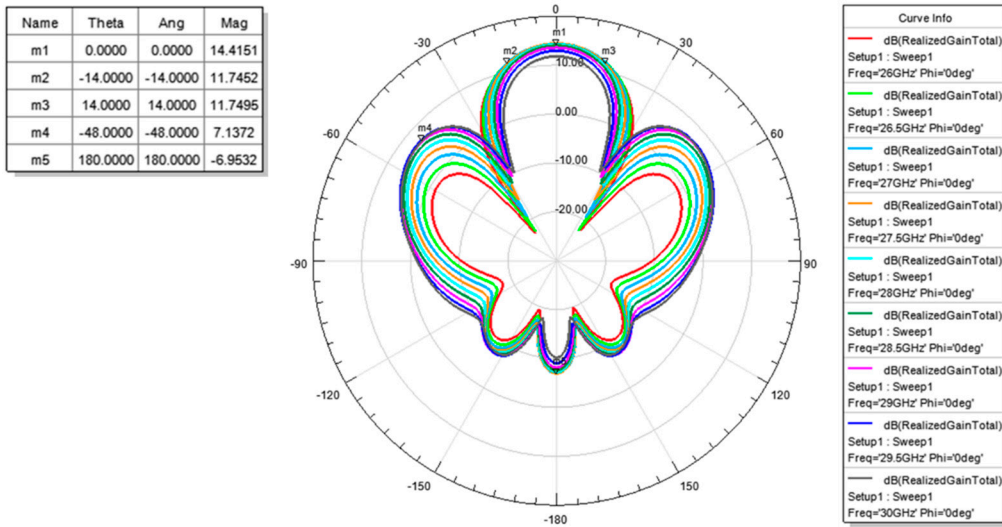**Figure 7.** Four (4) ports return loss of the simulation.

Name	Theta	Ang	Mag
m1	0.0000	0.0000	14.4151
m2	-14.0000	-14.0000	11.7452
m3	14.0000	14.0000	11.7495
m4	-48.0000	-48.0000	7.1372
m5	180.0000	180.0000	-6.9532

Figure 8. Radiation pattern of the simulation (X Cut).

Name	Theta	Ang	Mag
m1	0.0000	0.0000	14.4151
m2	-14.0000	-14.0000	11.7283
m3	14.0000	14.0000	11.7816
m4	-56.0000	-56.0000	4.9139
m5	180.0000	180.0000	-6.9396
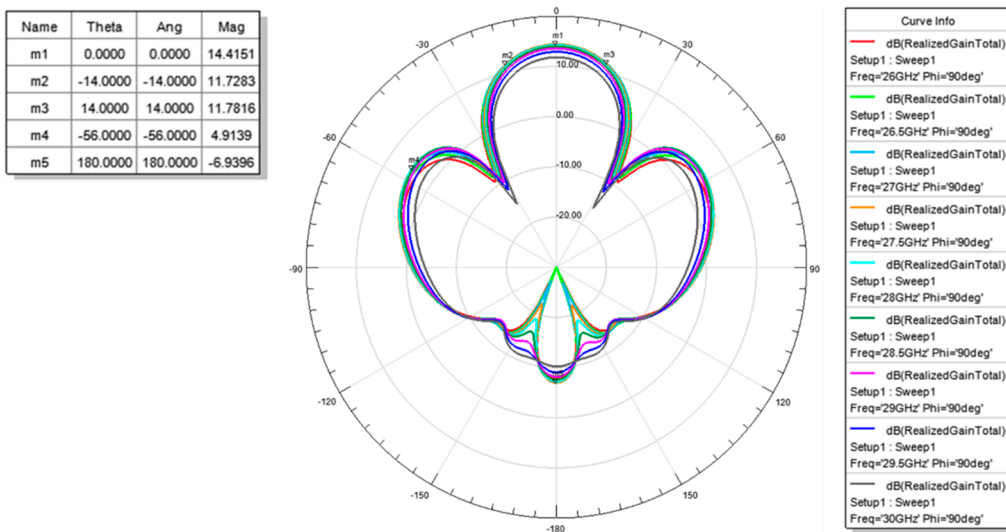
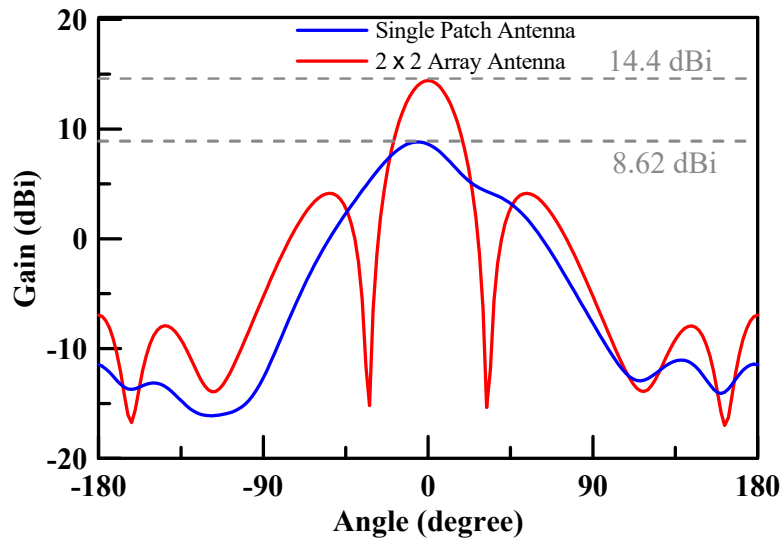**Figure 9.** Radiation pattern of the simulation (Y Cut).

Figure 10. Antenna peak gain.

The filed pattern of beam steering can be simulated by changing the phase of the four patch antennas. The simulation results of the beam steering tilted angle at 28 GHz are shown in Figures 11 and 12. The maximum gain was 14.4 dBi for both X cut and Y cut. The beam steering tilted angle was ±34° in the X cut while the beam steering tilted angle was ±26° in the Y cut.
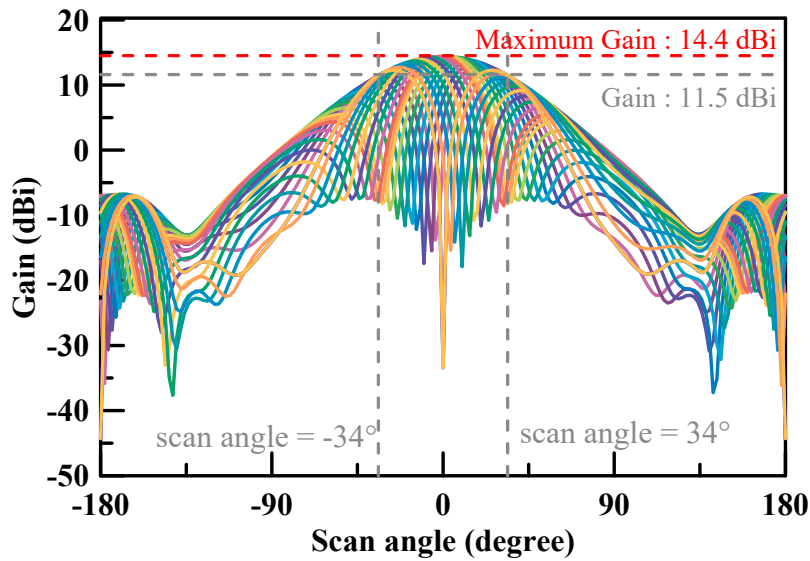

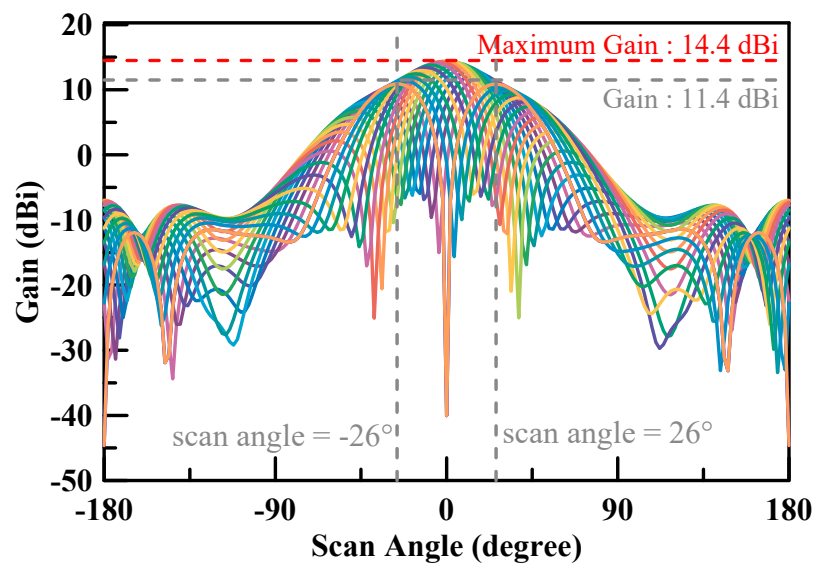**Figure 11.** Simulation results of the beam steering pattern at 28 GHz (X-cut).

Figure 12. Simulation results of the beam steering pattern at 28 GHz (Y-cut).

4. Antenna Manufacturing and Experimental Measurement

Progressive and lower loss materials were used to design a millimeter-wave antenna, such as Rogers (RO 4003C or RO 4350B), low temperature co-fired ceramics (LTCC), PTFE, and liquid crystal polymer (LCP). The manufacturing process of these novel kinds of materials is complex and their manufacturing costs are very expensive. The FR4 substrate has a lower cost compared to the other kinds of materials. The material cost of a Rogers material is three to five times more expensive than that of an FR4 material. Furthermore, the choice of the manufacturer, manufacturing quantity, design metal layers, and ordering options also affect the overall cost of the whole process. On the other hand, a low loss material process is 100 times more expensive than the manufacturing cost of a traditional FR4 PCB. However, the loss tangent of the low cost FR4 material is 0.01–0.04 at a frequency band of 26.5–29.5GHz, which restricts the performance of the antenna. The gain of the antenna that is designed on an FR4 substrate is approximately 4.5 dBi. The performance of the antenna that is designed on an FR4 substrate can be enhanced by using the air-filled cavity structure.

The antenna module proposed in this study was designed with a stack of three substrates and four metal layers (M1, M2, M3, and M4) as illustrated in Figure 13. The production process started by completing the circuit etching of the middle layer (M2 and M3) followed by the addition of two layers of PP (PP_1 and PP_2) on top and below the middle layer. During this step, the upper and lower materials of M2 (PP_1 and FR4_2) were laser precut as shown in the figure. The purpose of the laser precut is to leave a cutting path that will be used as a guide for the removal of the center substrate area later in the process. The next step was the lamination of M1 and M4, and the circuit etching for both metal layers. This was followed by creating laser holes from M1 to M2 and M3 to M4, and finally from M1 to M4. The final step involved mechanical drilling at the M4 surface towards the laser precut. Once the holes from the M4 surface to the laser precut were properly drilled and aligned, the center substrate could be removed therefore exposing the area of the entire air cavity. The key point of the process technology is on the air-filled cavity structure. The tolerance of each air-filled cavity must be made as small as possible. If the tolerance turned out to be significantly large, it will lead to a significant difference in the gain of each patch antenna. In turn, the performance of the array will be affected. In addition, the reserved M1 layer and its supporting material FR4_1 must be designed to be thin in order to have a lossless air-filled cavity. Moreover, if the air-filled cavity is too large in terms of area, it will have an impact on the antenna gain due to the changed distance of the patch relative to the ground.
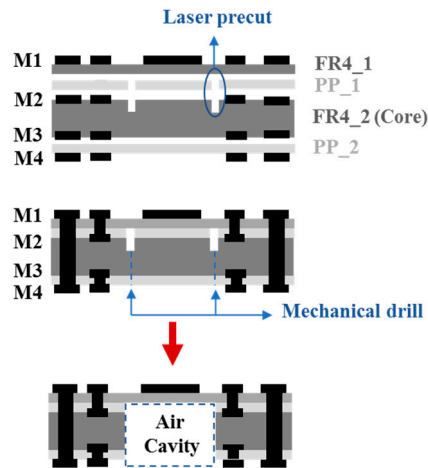
Figure 13. Manufacturing process of the antenna with an air-filled cavity.

The proposed array antenna was manufactured on an FR4 substrate. Figure 14 shows a photograph of the array antenna assembly. The measured results of the return loss for each port were better than 10 dB at an operating frequency band of 26.5–29.5 GHz. The comparison of the simulation and empirical results are presented in Figure 15. The empirical results are shown to satisfy the requirement of a 5G system millimeter wave band.
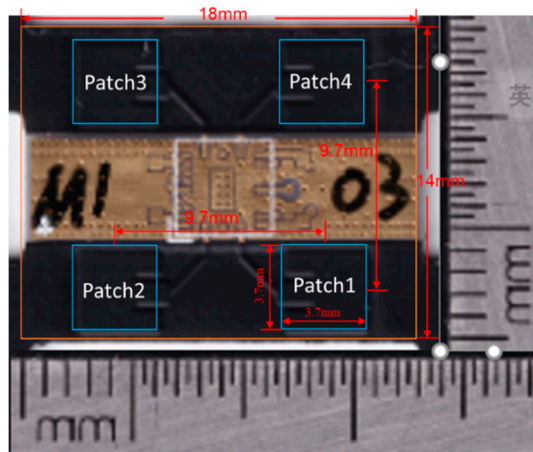

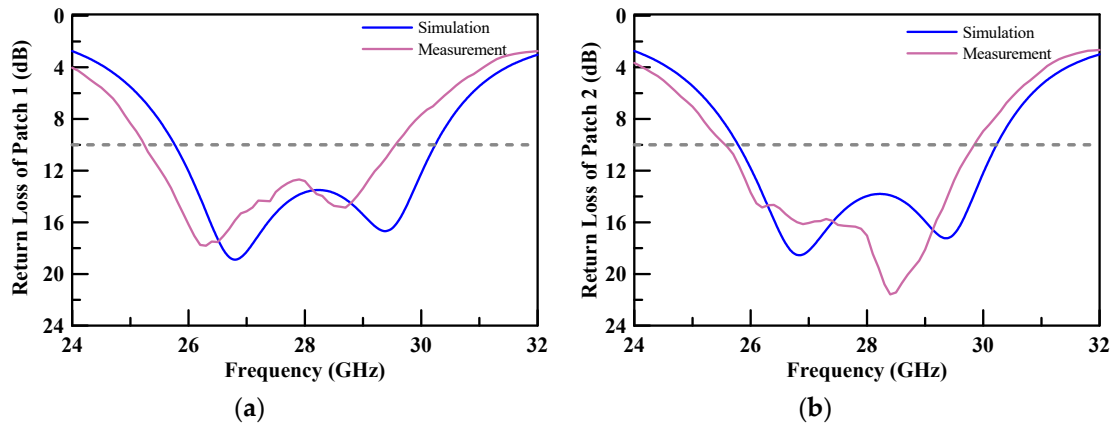**Figure 14.** Photograph of the array antenna (2 × 2).

(**a**)   (**b**)
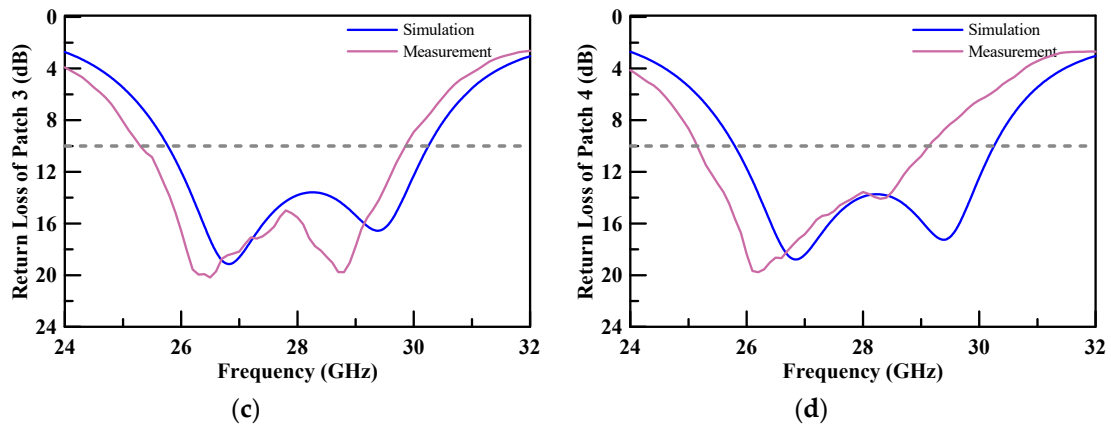
Figure 15. *Cont.*

Figure 15. Comparison of the simulation and empirical results of the return loss of each patch, (**a**) return loss of Patch1; (**b**) return loss of Patch2; (**c**) return loss of Patch3; (**d**) return loss of Patch4.

Figure 16 shows an NSI-700S-360 antenna chamber [26]. Its measurement coordinates are shown in Figure 17. The gain measurement results of each patch antenna are shown in Figure 18 (X-cut) and Figure 19 (Y-cut). The maximum gains were 8.58 dBi for Patch 1, 8.47 dBi for Patch 2, 8.49 dBi for Patch 3, and 8.64 dBi for Patch 4 in the X-cut. The maximum gain was 8.5 dBi for each Patch antenna in the Y-cut.
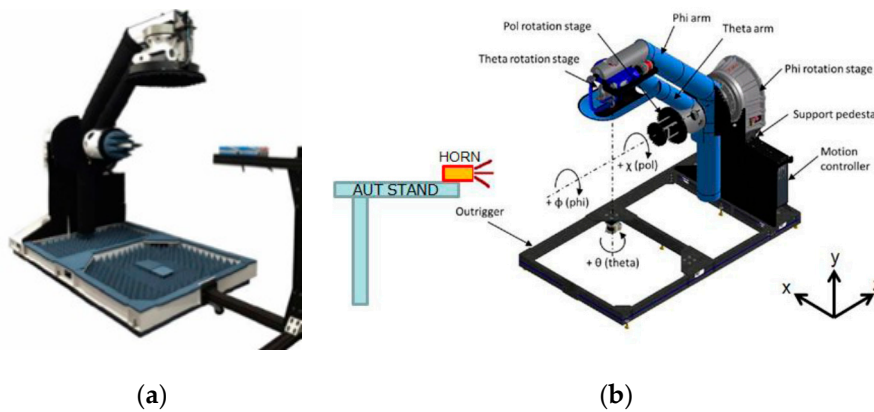

Figure 16. NSI-700S-360 antenna chamber, (**a**) instrument diagram; (**b**) equipment setup [26].
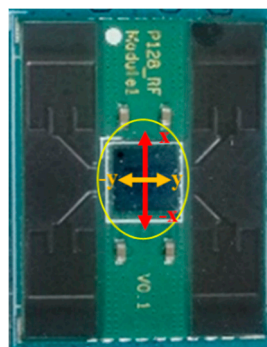

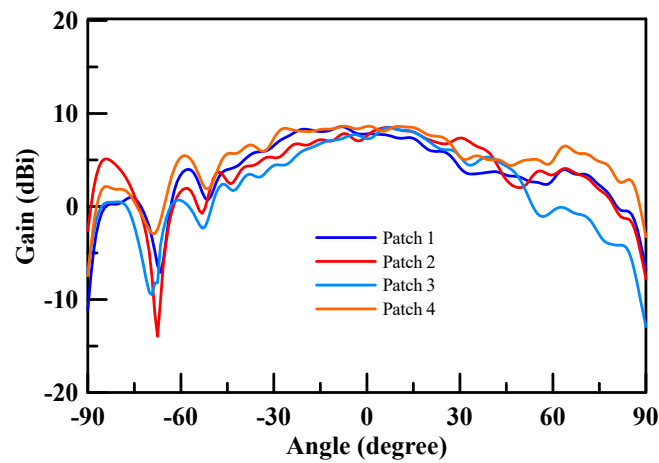**Figure 17.** Measurement coordinates.

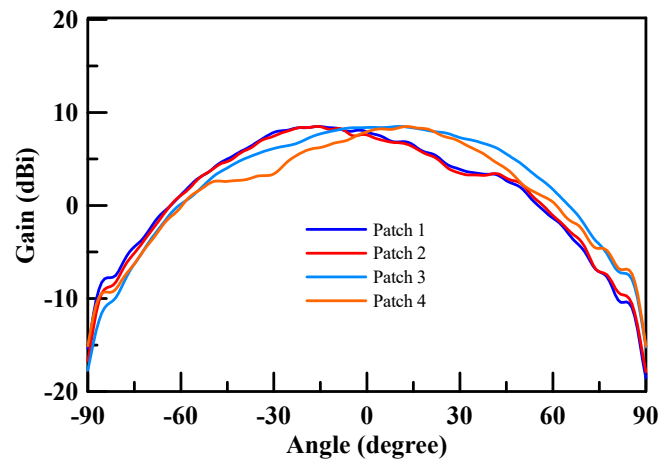**Figure 18.** Single patch antenna gain (X-cut).

Figure 19. Single patch antenna gain (Y-cut).

The gain measurement results of the array antenna are shown in Figures 20 and 21. The maximum gain was 14.4 dBi for the two cuts. The operated conditions of the phase for each patch antenna were Patch 1: 0 degree, Patch 2: 180 degree, Patch 3: 180 degree, and Patch 4: 0 degree. These results conform to the principle presented in Section 2. The 3D normalized radiation pattern is shown in Figure 22b, which shows similar 3D radiation patterns to the simulation results shown in Figure 22a.
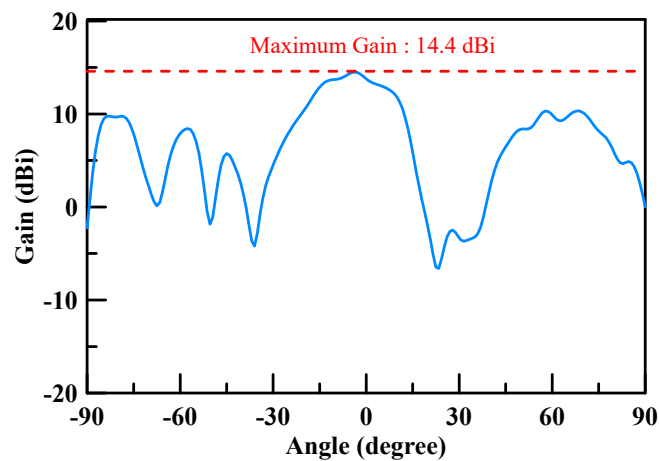

Figure 20. Array antenna (2 × 2) gain measurement results (phase 0/180/180/0, X-cut).
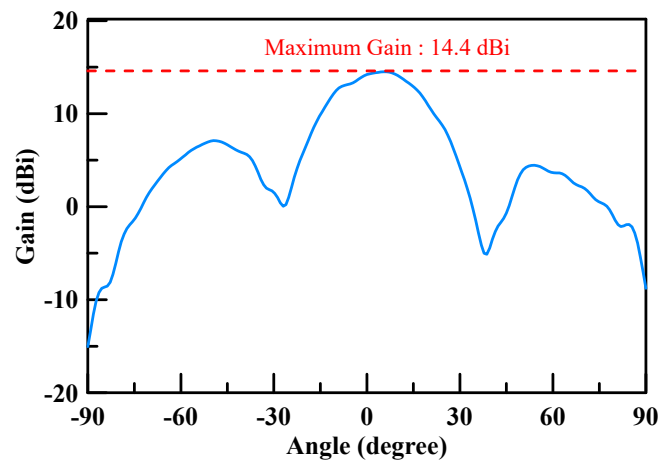
Figure 21. Array antenna (2 × 2) gain measurement results (phase 0/180/180/0, Y-cut).
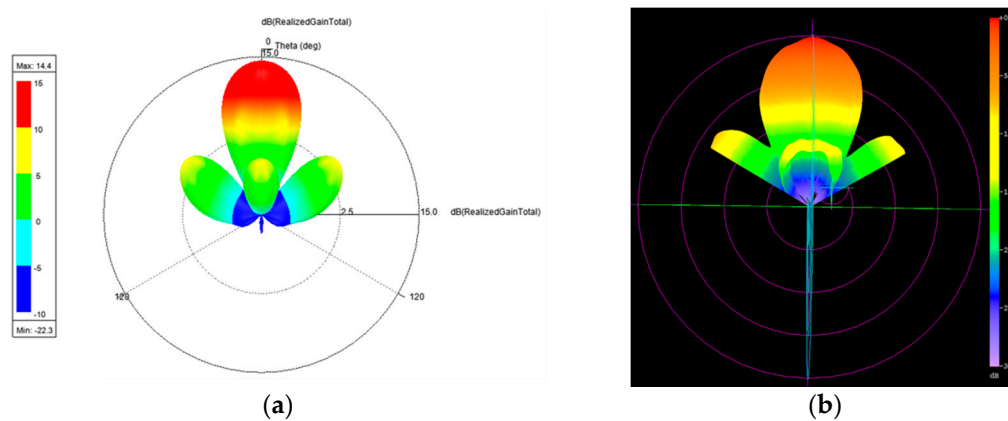

| (**a**) | (**b**) |

Figure 22. 3D radiation pattern of the array antenna at 28 GHz: (**a**) simulation result and (**b**) measurement result (normalized).

5. Conclusions

The design and simulation of a 2 × 2 low cost phase array antenna module for 5G applications operating at 28 GHz with 14.4 dBi antenna gain was proposed in this paper. The air-filled cavity used for patch antenna structure was with a FR4 PCB material for cost reduction instead of using a Roger or M6 material PCB. Moreover, it improved the antenna radiation efficiency by reducing the loss of the material. Furthermore, the designed array unit could be used and combined for a higher order array along two dimensions with a suitable surface mount technology (SMT) gap. It helps to easily and reliably implement a high order array. Therefore, the proposed array antenna is a promising candidate for the mm-wave 5G small cell applications. Table 2 summarizes the performance of this work and compares it with state-of-the-art mm-wave phased-array antennas [27–38]. The proposed patch shows around an 8.5 dBi antenna gain, which is better than [31,35,37,38], at a similar frequency. It describes that the air-filled cavity as a patch gap between the ground increased the antenna efficiency effectively instead of a lossy FR4 PCB material. The measured results of the single array unit show that the maximum radiation direction can be steered from −34 to +34° continuously in the X-cut and −26 to +26° continuously in the Y-cut at 28 GHz. The total dimension of the resulting design package was 18 mm × 14 mm × 0.71 mm. The gain of the array antenna achieved 14.4 dBi and the reflection coefficient of the array antenna was less than −10 dB from 26.5 to 29.5 GHz.

Table 2. Comparisons of antenna performance.

References	The Unit Cells Structure	The Bandwidth of Return Loss	The Peak Gain of the Array	Evaluated Peak Gain of the Unit Cell	The Dimensions of the Antenna Module	Material
[27]	2 × 2	9.2–10.8 GHz	7.5 dB 10.8–14 GHz	2.5dBi	112 mm × 112 mm	Rogers RT4735LZ
[28]	2 × 2	238.4–309.5 GHz	10.1 dB at 71.1 GHz	8 dBi	3×1.5 mm^2	silicon
[29]	4 × 4	57.2–64.5 GHz	6.9 dBi at 62 GHz	7.5 dBi	14 mm × 14 mm × 0.925 mm	Rogers 5880
[30]	4 × 4	12 GHz	8.9 dBi at 12 GHz	10.1 dBi	N/A	RO3003
[31]	1 × 8	27.2–29.2 GHz	10.33 dBi at 29.2 GHz	6 dBi	130 mm × 42 mm × 0.127 mm	Taconic RF-35
[32]	4 × 4	0.8 GHz	3.8 dBi at 30.5 GHz	6 dBi	6.85×6.85 cm^2	organic
[33]	2 × 2	N/A	4.5 dBi at 60 GHz	−1.5 dBi	4.5 mm × 3 mm	RO4003C
[34]	1 × 2	9.39–10.26 GHz	N/A	4.8 dBi (Simulated)	$15 \times 1\,5$ mm^2	RO4003
[35]	2 × 32 2 × 2 beamformer chips	23.5–30.5 GHz	EIRP 46 dBm	2~3 dBi	32 elements (5.3 mm) 2 × 2 beamformer (0.5 mm)	Megtron-6
[36]	2 × 2	N/A	15 dBi at 20 GHz	9 dBi	2 × 2 Quad-Mode Antenna Array (QMA)	N/A
[37]	Yagi–Uda antenna	26.86–28.87 GHz	6.03 dB at 26.86 GHz	6.03 dBi	25 mm × 15 mm	Rogers 5880
[38]	2 × 2 × 14	28–30 GHz	EIRP 54dBm	3~4 dBi	70 mm × 70 mm	N/A
This study	2 × 2	26.5~29.5 GHz	14.4 dB at 28 GHz	10.6 dBi	18 mm × 14 mm × 0.71 mm	FR4

Author Contributions: Conceptualization, W.-Y.C. and S.-L.C.; Data curation, W.-S.T., C.-K.L., P.-Z.R., and W.-M.C.; Formal analysis, C.-K.L., P.-Z.R., and W.-M.C.; Funding acquisition, W.-Y.C.; Investigation, W.-S.T. and W.-Y.C.; Methodology, W.-Y.C. and C.-K.L.; Project administration, P.-Z.R.; Resources, W.-Y.C., C.-A.C., P.A.R.A., and S.-L.C.; Supervision, C.-A.C., P.A.R.A., and S.-L.C.; Writing—original draft, W.-S.T., W.-Y.C., C.-A.C., and F.A.; Writing—review and editing C.-A.C., P.A.R.A., F.A., and S.-L.C. All authors have read and agreed to the published version of the manuscript.

Conflicts of Interest: The authors declare no conflict of interest.

References

1. Ateya, A.A.; Muthanna, A.; Gudkova, I.; Id, A.A.; Vybornova, A.; Koucheryavy, A. Development of Intelligent Core Network for Tactile Internet and Future Smart Systems. *J. Sens. Acuator Netw.* **2018**, *7*, 1. [CrossRef]
2. Szelag, B.; Drewnowski, J.; Łagód, G.; Majerek, D.; Dacewicz, E.; Fatone, F. Soft Sensor Application in Identification of the Activated Sludge Bulking Considering the Technological and Economical Aspects of Smart Systems Functioning. *Sensors* **2020**, *20*, 1941. [CrossRef] [PubMed]
3. Grasso, C.; Schembra, G. A Fleet of MEC UAVs to Extend a 5G Network Slice for Video Monitoring with Low-Latency Constraints. *J. Sens. Actuator Netw.* **2019**, *8*, 3. [CrossRef]
4. Patcharamaneepakorn, P.; Wu, S.; Wang, C.-X.; Aggoune, E.-H.M.; Alwakeel, M.M.; Ge, X.; Di Renzo, M.; Aggoune, H. Spectral, Energy, and Economic Efficiency of 5G Multicell Massive MIMO Systems With Generalized Spatial Modulation. *IEEE Trans. Veh. Technol.* **2016**, *65*, 9715–9731. [CrossRef]
5. Patcharamaneepakorn, P.; Wang, C.X.; Fu, Y.; Aggoune, E.H.M.; Alwakeel, M.M.; Tao, X.; Ge, X. Quadrature Space-Frequency Index Modulation Communication Systems. *IEEE Trans. Commun.* **2017**, *66*, 3050–3064. [CrossRef]
6. Kibaroglu, K.; Sayginer, M.; Rebeiz, G.M. A Low-Cost Scalable 32-Element 28-GHz Phased Array Transceiver for 5G Communication Links Based on a 2×2 Beamformer Flip-Chip Unit Cell. *IEEE J. Solid-State Circuits* **2018**, *53*, 1260–1274. [CrossRef]
7. Park, J.; Lee, S.Y.; Kim, J.; Park, D.; Choi, W.; Hong, W. An Optically Invisible Antenna-on-Display Concept for Millimeter-Wave 5G Cellular Devices. *IEEE Trans. Antennas Propag.* **2019**, *67*, 2942–2952. [CrossRef]
8. Kumar, P.; Urooj, S.; Malibari, A.A. Design of Quad-Port Ultra-Wideband Multiple-Input-Multiple-Output Antenna with Wide Axial-Ratio Bandwidth. *Sensors* **2020**, *20*, 1174. [CrossRef]
9. Ullah, S.; Ruan, C.; Sadiq, M.S.; Haq, T.U.; Fahad, A.K.; He, W. Super Wide Band, Defected Ground Structure (DGS), and Stepped Meander Line Antenna for Communication Applications. *Sensors* **2020**, *20*, 1735. [CrossRef]
10. Hamberger, G.F.; Trummer, S.; Siart, U.; Eibert, T.F. A Planar Dual-Polarized Microstrip 1-D-Beamforming Antenna Array for the 24-GHz Band. *IEEE Trans. Antennas Propag.* **2016**, *65*, 142–149. [CrossRef]
11. Chiang, W.-Y.; Ku, C.-H.; Chen, C.-A.; Wang, L.-Y.; Abu, P.A.; Rao, P.-Z.; Liu, C.-K.; Liao, C.-H.; Chen, S.-L. A Power-Efficient Multiband Planar USB Dongle Antenna for Wireless Sensor Networks. *Sensors* **2019**, *19*, 2568. [CrossRef] [PubMed]
12. Chen, S.-L.; Lee, H.-Y.; Chen, C.-A.; Huang, H.-Y.; Luo, C.-H. Wireless Body Sensor Network with Adaptive Low-Power Design for Biometrics and Healthcare Applications. *IEEE Syst. J.* **2009**, *3*, 398–409. [CrossRef]
13. Chen, C.-A.; Chen, S.-L.; Huang, H.-Y.; Luo, C.-H. An Asynchronous Multi-Sensor Micro Control Unit for Wireless Body Sensor Networks (WBSNs). *Sensors* **2011**, *11*, 7022–7036. [CrossRef]
14. Wang, L.-H.; Zhang, W.; Guan, M.-H.; Jiang, S.-Y.; Fan, M.-H.; Abu, P.A.; Chen, C.-A.; Chen, S.-L. A Low-Power High-Data-Transmission Multi-Lead ECG Acquisition Sensor System. *Sensors* **2019**, *19*, 4996. [CrossRef] [PubMed]
15. Chen, C.-A.; Wu, C.; Abu, P.A.; Chen, S.-L. VLSI Implementation of an Efficient Lossless EEG Compression Design for Wireless Body Area Network. *Appl. Sci.* **2018**, *8*, 1474. [CrossRef]
16. Chen, C.-A.; Chen, S.-L.; Huang, H.-Y.; Luo, C.-H. An Efficient Micro Control Unit with a Reconfigurable Filter Design for Wireless Body Sensor Networks (WBSNs). *Sensors* **2012**, *12*, 16211–16227. [CrossRef]
17. Chen, S.-L.; Wu, G.-S. A Cost and Power Efficient Image Compressor VLSI Design with Fuzzy Decision and Block Partition for Wireless Sensor Networks. *IEEE Sens. J.* **2017**, *17*, 4999–5007. [CrossRef]
18. Chen, S.-L. A Power-Efficient Adaptive Fuzzy Resolution Control System for Wireless Body Sensor Networks. *IEEE Access* **2015**, *3*, 743–751. [CrossRef]
19. Chen, S.-L.; Tuan, M.-C.; Lee, H.-Y.; Lin, T.-L. VLSI Implementation of a Cost-Efficient Micro Control Unit with an Asymmetric Encryption for Wireless Body Sensor Networks. *IEEE Access* **2017**, *5*, 4077–4086. [CrossRef]
20. Taylor, W.; Shah, S.A.; Dashtipour, K.; Zahid, A.; Abbasi, Q.; Imran, M. An Intelligent Non-Invasive Real-Time Human Activity Recognition System for Next-Generation Healthcare. *Sensors* **2020**, *20*, 2653. [CrossRef]
21. "3GPP Specification Series: 38series". 3GPP. Available online: https://www.3gpp.org/DynaReport/38-series.htm (accessed on 22 February 2019).
22. David, K.C. *Field and Wave Electromagnetics*, 2nd ed.; Addison-Wesley Publishing Company: Reading, MA, USA, 1989.

23. Tung, W.-S.; Rao, P.-Z.; Chen, W.-M. A millimeter-wave antenna on low cost FR4 substrate. In Proceedings of the 2019 IEEE Asia-Pacific Microwave Conference (APMC), Singapore, 10–13 December 2019.

24. Roy, J.S. Multiple-Antenna Techniques in Wireless Communication-Technical Aspects. *Int. J. Inf. Commun. Technol. Digit. Converg.* **2016**, *1*, 24–32.

25. Stutzman, W.L.; Thiele, G.A. *Antenna Theory and Design*, 3rd ed.; John Wiley & Sons Inc.: Hoboken, NJ, USA, 2012.

26. Henderson, R.; Pierce, R.; Aroor, S.; Arzola, J.; Miller, C.; Kumar, H.; Ei, T.; Blanchard, A.; Fooshe, D.; Schluper, B.; et al. Millimeter-wave performance of broadband aperture antenna on laminates. In Proceedings of the AMTA 2015, Long Beach, CA, USA, 11–16 October 2015.

27. Fan, Y.; Wang, J.; Li, Y.; Zhang, J.; Han, Y.; Qu, S. Low-RCS and High-Gain Circularly Polarized Metasurface Antenna. *IEEE Trans. Antennas Propag.* **2019**, *67*, 7197–7203. [CrossRef]

28. Chang, L.; Li, Y.; Zhang, Z.; Wang, S.; Feng, Z. Planar Air-Filled Terahertz Antenna Array Based on Channelized Coplanar Waveguide Using Hierarchical Silicon Bulk Micromachining. *IEEE Trans. Antennas Propag.* **2018**, *66*, 5318–5325. [CrossRef]

29. Zhang, T.; Li, L.; Xie, M.; Xia, H.; Ma, X.; Cui, T.J. Low-Cost Aperture-Coupled 60-GHz-Phased Matching Network. *IEEE Trans. Antennas Propag.* **2017**, *65*, 6355–6362. [CrossRef]

30. Zhang, T.; Li, L.; Xia, H.; Ma, X.; Cui, T.J. A Low-Cost and High-Gain 60-GHz Differential Phased Array Antenna in PCB Process. *IEEE Trans. Compon. Packag. Manuf. Technol.* **2018**, *8*, 1281–1291. [CrossRef]

31. Lee, H.; Kim, S.; Choi, J. A 28 GHz 5G Phased Array Antenna with Air-Hole Slots for Beam Width Enhancement. *Appl. Sci.* **2019**, *9*, 4204. [CrossRef]

32. Liu, D.; Gu, X.; Baks, C.W.; Valdes-Garcia, A. Antenna-in-Package Design Considerations for Ka-Band 5G Communication Applications. *IEEE Trans. Antennas Propag.* **2017**, *65*, 6372–6379. [CrossRef]

33. Baniya, P.; Bisognin, A.; Sain, A.; Luxey, C. Chip-to-Chip Switched Beam 60 GHz Circular Patch Planar Antenna Array and Pattern Considerations. *IEEE Trans. Antennas Propag.* **2018**, *66*, 1776–1787. [CrossRef]

34. Kaouach, H. Wideband high-efficiency unit-cell for 1-bit and 2-bit transmit-arrays operating in X-band. In Proceedings of the 11th European Conference on Antennas and Propagation (EUCAP), Paris, France, 19–24 March 2017; pp. 2320–2324.

35. Ma, Q.; Chung, H.; Yin, Y.; Kanar, T.; Zihir, S.; Rebeiz, G.M. A 5G 24-30 GHz 2 × 32 element dual-polarized dual-beam phased array base-station for 2x2 MIMO systems. In Proceedings of the 2019 IEEE Global Communications Conference (GLOBECOM), Waikoloa, HI, USA, 9–13 December 2019; pp. 1–5.

36. Van Tonder, G.; Meyer, P. Beamforming Techniques for a Quad-Mode Antenna Array. In Proceedings of the 13th European Conference on Antennas and Propagation (EuCAP), Krakow, Poland, 31 March–5 April 2019; pp. 1–4.

37. Shu, J.; Xu, G.; Peng, H.; Mao, J. An Electrically Steerable Parasitic Array Radiator in Package Based on Liquid Crystal. *IEEE Trans. Antennas Propag.* **2019**, *18*, 2365–2369. [CrossRef]

38. Valdes-Garcia, A.; Sadhu, B.; Gu, X.; Tousi, Y.; Liu, D.; Reynolds, S.K.; Haillin, J.; Sahl, S.; Rexberg, L. Circuit and antenna-in-package innovations for scaled mmWave 5G phased array modules. In Proceedings of the 2018 IEEE Custom Integrated Circuits Conference (CICC), San Diego, CA, USA, 8–11 April 2018; pp. 1–8.